48th AIAA Aerospace Sciences Meeting Including the New Horizons Forum and Aerospace Exposition
4 - 7 January 2010, Orlando, Florida

AIAA 2010-254

Active Aerodynamic Blade Distributed Flap Control Design Procedure for Load Reduction on the UpWind 5MW Wind Turbine

David G. Wilson*, Brian R. Resor†, Dale E. Berg‡
Sandia National Laboratories, P.O. Box 5800, Albuquerque, NM 87185
Thanasis K. Barlas§, Gijs A.M. van Kuik¶
Delft University of Technology, Delft, The Netherlands

This paper develops a system identification approach and procedure that is employed for distributed control system design for large wind turbine load reduction applications. The primary goal of the study is to identify the process that can be used with multiple sensor inputs of varying types (such as aerodynamic or structural) that can be used to construct state-space models compatible with MIMO modern control techniques (such as LQR, LQG, H_∞, robust control, etc.). As an initial step, this study employs LQR applied to multiple flap actuators on each blade as control inputs and local deflection rates at the flap spanwise locations as measured outputs. Future studies will include a variety of other sensor and actuator locations for both design and analysis with respect to varying wind conditions (such as high turbulence and gust) to help reduce structural loads and fatigue damage. The DU_SWAMP aeroservoelastic simulation environment is employed to capture the complexity of the control design scenario. The NREL 5MW UpWind reference wind turbine provides the large wind turbine dynamic characteristics used for the study. Numerical simulations are used to demonstrate the feasibility of the overall approach. This study shows that the distributed controller design can provide load reductions for turbulent wind profiles that represent operation in above-rated power conditions.

Nomenclature

$\mathbf{Y}$	observer Markov parameter
$\mathbf{H}$	generalized Hankel matrix
$\mathbf{x}$	state vector
$\mathbf{y}$	output vector
$\mathbf{u}$	input (or control) vector
$\mathbf{A}$	state matrix
$\mathbf{B}$	input matrix
$\mathbf{C}$	output matrix
$\mathbf{D}$	direct feedthrough matrix
$\mathbf{G}$	forward observer gain matrix
$\mathbf{K}$	state feedback control gain matrix
$\mathbf{v}$	observer output vector
J	performance index
$\mathbf{u}_{max}$	maximum control effort vector
$\mathbf{v}_{max}$	maximum sensor output vector

*Technical Staff, Energy Systems Analysis/Wind and Water Power Technologies Department; dwilso@sandia.gov, MS 1108
†Technical Staff, Wind and Water Power Technologies Department; brresor@sandia.gov, MS 1124
‡Technical Staff, Wind and Water Power Technologies Department; deberg@sandia.gov, MS 1124
§Ph.D. Researcher, Wind Energy; Faculty of Aerospace Engineering; Kluyverweg 1, 2629 HS; a.barlas@tudelft.nl
¶Professor, Wind Energy; Faculty of Aerospace Engineering; Kluyverweg, 1, 2629 HS; g.a.m.vankuik@tudelft.nl

I. Introduction

Wind turbines are large, complex dynamically flexible structures that operate in turbulent and unpredictable environmental conditions where efficiency and reliability are highly dependent upon a well-designed control strategy. The possibility to quickly influence aerodynamic loads acting on the individual blades allows for a hybrid pitch control objective that includes a high frequency dynamic attenuation component with respect to fatigue load reduction. Active aerodynamic devices are potential candidates for this component. With the increasing size of wind turbine blades, the need for more sophisticated load control techniques has induced interest in locally distributed aerodynamic control systems (e.g. trailing edge flaps) with built-in intelligence on the blades (such as smart structures). Several researchers have started to investigate the benefits of using advanced control for wind turbine rotor aerodynamics and geometry. In McCoy and Griffin,[1] two major categories of rotor aerodynamic modifications were investigated; active aerodynamic devices and actively controlled retractable blade rotors. Both studies indicated cost savings through reduced system loads and increased energy capture. There are various options for utilizing active distributed flaps along the blade span for load reduction. Van Dam et. al.,[2–4] have investigated, both computationally with CFD investigations and through experimental wind tunnel testing, the feasibility of using microtabs for active load control. Andersen, et.al.[5] have developed deformable trailing edge geometry and control algorithms which also showed fatigue load reduction for both the flapwise blade root moments and the tower root moments. By enabling the trailing edge at the outboard portion of the blade to move quickly and independently, local fluctuations in the aerodynamic forces can be compensated. In Barlas and van Kuik[6] an overview of smart rotor control technology for wind turbines is given.

Most recently, Barlas and van Kuik[7] have employed a new aeroservoelastic tool to evaluate varying single and multi-flap per each blade control strategies that primarily concentrate on Singe-Input Single-Output (SISO) Proportional-Integral-Derivative (PID) style distributed flap control systems as a proof-of-concept. This paper presents a modern Multi-Input Multi-Output (MIMO) control system design procedure based on distributed flap actuation and appropriate sensor feedback along the outboard of each blade that seamlessly integrates with a blade independent pitch control strategy. This modern controller design is modeled and analyzed with the new state-of-the-art comprehensive aeroservoelastic simulator, called DU_SWAMP,[7] which is implemented in the Matlab/Simulink environment.[8] In addition, this paper builds upon recent developments in Active Aerodynamic Load Control (AALC) strategies currently being investigated at Sandia National Laboratories Wind and Water Power Technologies department.[9–14]

A. The DU_SWAMP Aeroservoelastic Simulation Tool

DU_SWAMP[7] has been developed at Delft University Wind Energy Research Institute (DUWIND) and simulates a full aeroservoelastic wind turbine model including all possible control options. The structure of the code is fully modular, which offers the possibility to easily adapt the model configuration and complexity by interchanging modules. The implementation of additional features like trailing edge flap aerodynamics or actuator dynamics is also facilitated. A flexible multi-body representation of the structural dynamics of the wind turbine, by means of the superelement approach, is used. The normal BEM aerodynamic model has been extended with airfoil section unsteady aerodynamics including the effect of the active flaps. All normal wind input disturbances are included. The distributed trailing edge flaps are implemented as active aerodynamic load control devices on the UpWind 5MW wind turbine.[15]

B. The NREL 5MW Reference Turbine

A full description of the NREL 5MW Offshore turbine model can be found in reference.[15] The turbine model provides detailed specifications of a large wind turbine that is representative of typical utility-scale land- and sea-based multi-megawatt turbines, and is suitable for deployment in deep waters. The wind turbine is a conventional three-bladed upwind variable-speed variable blade-pitch-to-feather-controlled turbine. Figure 1 summarizes the most basic properties of the model used in this investigation.

DU_SWAMP has the capability to model structural torsion in the blades and tower. However, this feature is not exercised in the current investigation. The current DU_SWAMP model accurately represents the first and second structural modes in each orthogonal direction for both the tower and the blades. The following additional physics are not included in the current investigation: drive train dynamics, tower shadow, and aerodynamic hub losses.

Rating	5.0 MW
Rotor Diameter	126 m
Hub Height	90 m
Tower Length	107.6 m (offshore baseline monopile tower with rigid foundation)
Cut-In, Rated, Cut-Out Wind Speeds	3 mps, 11.4 mps, 25 mps
AALC Device	Conventional Flap (10% chord)
Extent of Flap (DU_SWAMP: Three discrete flaps/blade)	~67% to 91% of blade span, 25% of blade radius
Deflection and rate limits	+/- 10 degrees, +/- 100 degrees/second (Rule-of-thumb)

Figure 1. NREL 5MW UpWind offshore reference turbine model characteristics

C. Process for System Identification and Control Design

This paper demonstrates a process for system identification and MIMO control design of an operating wind turbine. System identification of an operating wind turbine, as opposed to the parked wind turbine structure, is meaningful in that it accounts for dynamic effects due to rotor rotation and aerodynamic loads and damping. A challenge in system identification of an operating wind turbine is in designing inputs that excite the dynamics of interest in the turbine structure.

This work is meant to present the major steps required to adequately characterize a nonlinear aeroservoelastic system during operation and design a control scheme that includes effects of the most important dynamics contributing to system behavior. The process demonstrated here is equally useful for numerical simulation of aerodynamically loaded wind turbines and for characterization and control design of a real wind turbine with active aerodynamic devices. An advantage of numerical simulation is the easy access to simulated sensors for input and output purposes. A disadvantage of numerical simulation is the degree of confidence in the physical models and assumptions that are used in the simulation. A simulation tool such as DU_SWAMP provides the opportunity to prove out processes prior to field implementation. The DU_SWAMP model is believed to include higher fidelity structural and aerodynamic models, e.g. unsteady aerodynamic active flap models, that what are typically available in similar wind turbine system codes.[9]

A summary of the process follows: Section II of this paper outlines the procedure for system identification, resulting in a state-space model compatible for MIMO controller design. Section III introduces the MIMO modern control design approach. In Section IV, numerical simulation results are given for the modern MIMO control design validation. In final Section V the paper results and future directions are given.

The steps outlined below in this paper are not carried out to their full potential at the present time. The value in demonstration of the process is in identification of the important challenges inherent to application of the techniques to a large scale turbine. Future work will deal with the challenges in a more focused manner and will design optimized controllers which have the ability to affect the dynamics of a system in a highly efficient manner.

II. System Identification using OKID/ERA

The state-space model continues to receive substantial attention for system analysis and design of feedback control systems. Many aerospace applications, such as large space structures and aircraft, have benefited.[16–19] A mathematical model that adequately captures the systems dynamical motion is necessary for a successful controller design. System realization is the process of building a state-space model from experimental data and is an integral part of system identification and model accuracy.[20]

The aeroservoelastic wind simulator, DU_SWAMP, provides time histories of the variables of the aeroservoelastic 5MW turbine model. However, an explicit mathematical model is not generated for the system. Therefore, a control design mathematical model of a *computational aeroservoelastic system* is developed.

The method of identifying the plant models, as well as the process and sensor noise statistics, chosen for this study was the Observer/Kalman filter IDentification (OKID) method.[20–22] This method of system identification uses only input and output data to construct a discrete-time state-space realization of the system. The OKID method is well suited for MIMO systems and by definition, the generated model matches the output in a least squares sense.[21]

The OKID algorithm includes an observer in the system identification process. The first step in the process calculates the observer Markov parameters determined as[21,23]

$$\mathbf{Y}_0 = \mathbf{D}, \quad \mathbf{Y}_1 = \mathbf{CB}, \quad \mathbf{Y}_2 = \mathbf{CAB}, \quad \ldots, \quad \mathbf{Y}_k = \mathbf{CA}^{k-1}\mathbf{B}$$

where these Markov parameters are assembled into the generalized Hankel matrix[21,23]

$$\mathbf{H}_{k-1} = \begin{bmatrix} \mathbf{Y}_k & \mathbf{Y}_{k+1} & \ldots & \mathbf{Y}_{k+\beta-1} \\ \mathbf{Y}_{k+1} & \mathbf{Y}_{k+2} & \ldots & \mathbf{Y}_{k+\beta} \\ \vdots & \vdots & \ddots & \vdots \\ \mathbf{Y}_{k+\alpha-1} & \mathbf{Y}_{k+\alpha} & \ldots & \mathbf{Y}_{k+\alpha+\beta-1} \end{bmatrix} = \begin{bmatrix} \mathbf{C} \\ \mathbf{CA} \\ \mathbf{CA}^2 \\ \vdots \\ \mathbf{CA}^{\alpha-1} \end{bmatrix} \mathbf{A}^{k-1} \begin{bmatrix} \mathbf{B} & \mathbf{AB} & \mathbf{A}^2\mathbf{B} \ldots \mathbf{A}^{\beta-1}\mathbf{B} \end{bmatrix}.$$

The next step employs a least squares technique to compute the system Markov parameters from which the observability, controllability, and state transition matrices can be determined.[21] In the final step the Markov parameters are used to generate the discrete-time state-space model via the Eigensystem Realization Algorithm (ERA). A Singular Value Decomposition (SVD) is employed to truncate the Hankel matrix by reconstructing the triplet $(\mathbf{A}, \mathbf{B}, \mathbf{C})$ into a balanced realization (equivalent controllability and observability Grammians). The discrete-time state-space model (**A,B,C,D**) to be identified defines the relationship between the r-vector driving excitation (multi-flap) inputs $\mathbf{u}_k$ and the measurement m-vector (local deflection, local deflection rate, or other measurement) outputs $\mathbf{y}_k$ given as[21,23]

$$\begin{aligned} \mathbf{x}_{k+1} &= \mathbf{A}\mathbf{x}_k + \mathbf{B}\mathbf{u}_k \\ \mathbf{y}_k &= \mathbf{C}\mathbf{x}_k + \mathbf{D}\mathbf{u}_k \end{aligned}$$

For the demonstration case, the controller regulates the local flap deflection rate output (m=3) for each flap control input (r=3). Therefore, the sensor measurement includes the local flap deflection rate for each flap (three individual flaps per blade). At this point an observer is added to the linear system equations through the following transformation[21,23]

$$\begin{aligned} \mathbf{x}_{k+1} &= \mathbf{A}\mathbf{x}_k + \mathbf{B}\mathbf{u}_k + (\mathbf{G}\mathbf{y}_k - \mathbf{G}\mathbf{y}_k) \\ &= [\mathbf{A} + \mathbf{GC}]\,\mathbf{x}_k + [\mathbf{B} + \mathbf{GD}]\,\mathbf{u}_k - \mathbf{G}\mathbf{y}_k \\ &= \hat{\mathbf{A}}\mathbf{x}_k + \hat{\mathbf{B}}\mathbf{v}_k \end{aligned}$$

where

$$\hat{\mathbf{A}} \equiv [\mathbf{A} + \mathbf{GC}], \quad \hat{\mathbf{B}} \equiv [\mathbf{B} + \mathbf{GD} \quad -\mathbf{G}] \quad \text{and} \quad \mathbf{v}_k \equiv [\mathbf{u}_k \quad \mathbf{y}_k]^T.$$

The system stability is established through augmentation of the ideal Markov parameters with the observer.[23]

Initially, the DU_SWAMP model is driven with a constant and steady wind of 15 m/s. Excitation signals are applied individually to each of the three trailing edge flaps on each blade. The excitation signal consists of a sinusoidal chirp (see Fig. 2 left) starting at 0.01 Hz and ending at 2.5 Hz with an amplitude and duration of ±15 degrees for 200 seconds, respectively. The chirp frequency varies linearly with time. The corresponding local deflection rate for the first flap is shown in Fig. 2 (right). Similar responses exist for the other flaps in the system.

Six open-loop data sets were created from applying different combinations of chirp signals as inputs and record sensor responses as outputs. Three sets included a single flap input per each blade. The last three sets included combinations of the three flaps per each blade. In all cases, the same signals to each respective multi-flap was applied to each respective blade symmetrically. For this set of data there was not any antisymmetric scenarios investigated. For future work, by increasing the data set to include antisymmetric scenarios other system wind turbine antisymmetric modes may be identified. These data files are used as input by OKID to identify the dynamic characteristics of the model. The number of actual modes identified become a function of the richness of excitation in the data sets.

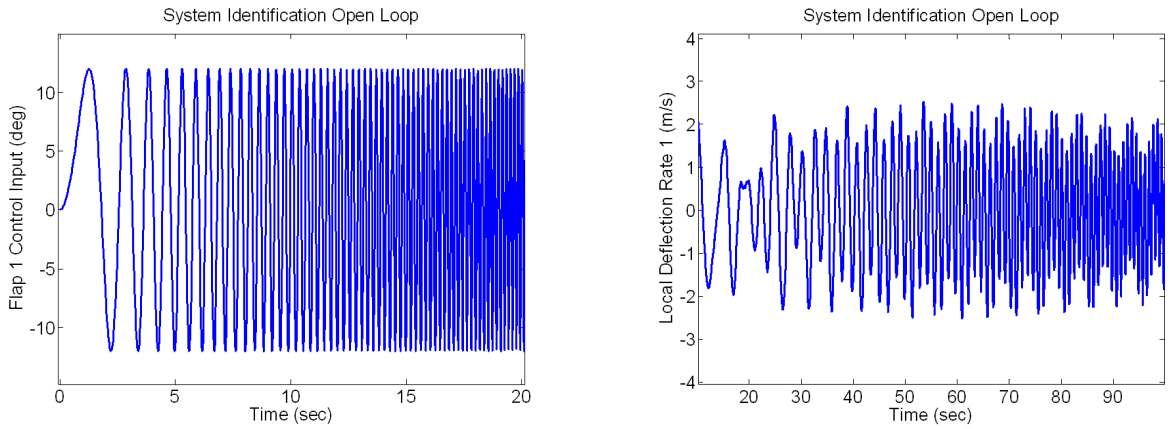

Figure 2. Multi-flap excitation open-loop sinusoidal chirp signal (left) and corresponding local deflection rate response (right)

The input for OKID[22] requires the data sets and an estimated number of observer Markov parameters to be solved for specified. Several different selections were tried and for $p = 20$ the results of the OKID model fitting are shown in Fig. 3 for the Hankel matrix singular value decomposition. The first two modes

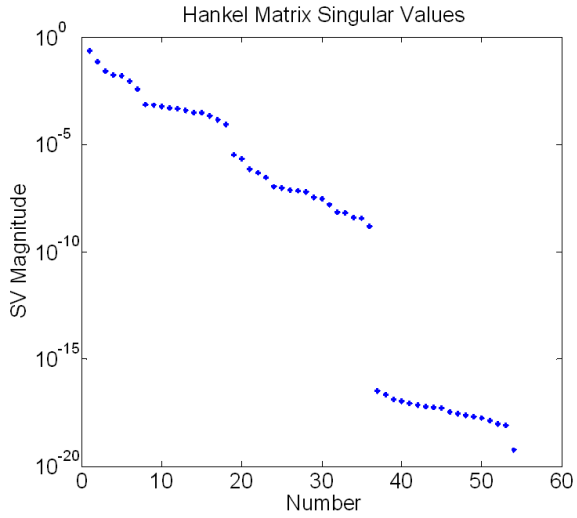

Figure 3. Hankel matrix singular value (retained first two modes)

are retained in the derived model and the remaining modes truncated. Other options within the OKID process can help better identify which modes are real and which are artifical computation modes, however, in the final selection of the model, engineering judgement plays a large role. For future applications many different runs and variations will help to identify further modes and characteristics. The two modes retained are 0.647 Hz and 2.05 Hz, respectively. These most closely resemble the 1^{st} blade collective flap and 2^{nd} blade collective flap modes from[15] (0.6675 Hz and 2.0205 Hz). Note that these modal frequencies[15] are derived from a linearized analysis and do not include aerodynamic damping and/or the effects of the applied aerodynamic forces. In contrast to the OKID model which is derived in steady-state wind conditions and excitations applied to external blade actuation. In future work, this will help to define a specific set of analyses and tests to be applied that best identify actual modal values, characteristic of system dynamics, that the wind turbine is experiencing in represenative *real life* scenarios. The corresponding observer match with actual responses in Fig. 4 (left) and close-up trace (right). The errors in the model match are on the order of (10^{-5}). The resulting observer model is employed by the controller design, discussed next.

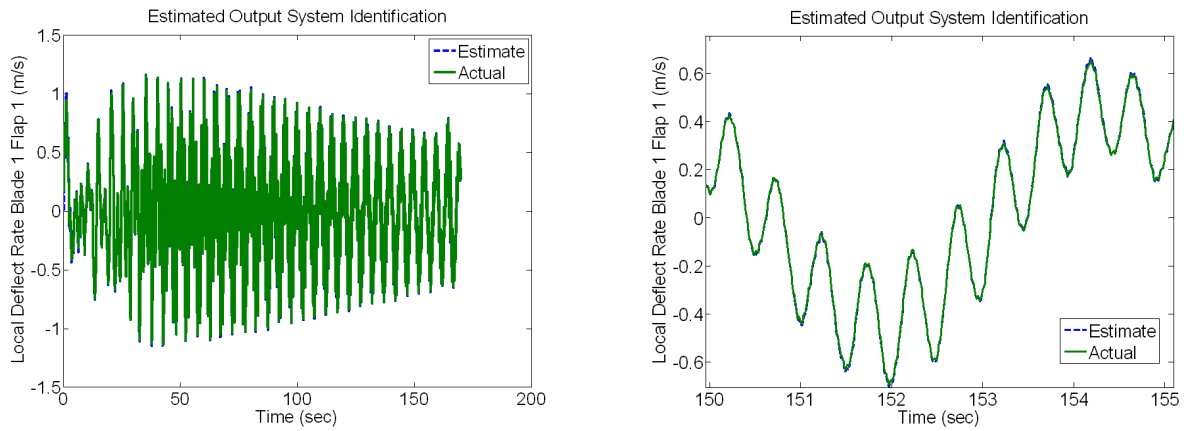

Figure 4. Estimated and true output responses (left) including detailed blow-up section (right)

III. Preliminary MIMO LQR Flap Control Design

The last step in the process is to design the closed-loop feedback controller. The controller was designed using standard LQR methodology[24] coupled with the identified state estimator from the OKID method.[21] The LQR controller determined from the quadratic cost[16, 23, 24]

$$J = \sum_{k=0}^{\infty} \left(\mathbf{x}_k^T \mathbf{C}^T \begin{bmatrix} \frac{1}{v_{max_1}^2} & 0 & 0 \\ 0 & \frac{1}{v_{max_2}^2} & 0 \\ 0 & 0 & \frac{1}{v_{max_3}^2} \end{bmatrix} \mathbf{C}\mathbf{x}_k + \mathbf{u}_k^T \begin{bmatrix} \frac{1}{u_{max_1}^2} & 0 & 0 \\ 0 & \frac{1}{u_{max_2}^2} & 0 \\ 0 & 0 & \frac{1}{u_{max_3}^2} \end{bmatrix} \mathbf{u}_k \right)$$

minimizes the weighted sum of $\mathbf{v}_{max} = [0.9\ 0.9\ 0.9]^T$ m/s and $\mathbf{u}_{max} = [20\ 20\ 20]^T$ degrees which are treated as the design parameters. The solution to the LQR minimization is the resulting state feedback gain matrix $\mathbf{K}$. Given that the implementation includes the OKID estimator, then at any given time-step, the control law is calculated from the current estimate as[16, 23, 24]

$$\mathbf{u}_k = -\mathbf{K}\hat{\mathbf{x}}_k$$

and the estimator is propagated forward in time using the current control and measured system outputs as[16, 23, 24]

$$\hat{\mathbf{x}}_{k+1} = [\mathbf{A} + \mathbf{GC}]\,\hat{\mathbf{x}}_k + [\mathbf{B} + \mathbf{GD}]\,\mathbf{u}_k - \mathbf{G}\mathbf{y}_k$$

where $\hat{\mathbf{x}}_{k+1}$ is the future state estimate, $\hat{\mathbf{x}}_k$ the current state estimate, $\mathbf{u}_k$ current flap actuator command, and $\mathbf{y}_k$ the current sensor (local flap deflection rate) measurements. This formulation was implemented in the flap control module in DU_SWAMP and numerical simulations conducted to test the performance.

IV. Numerical Simulation Results and Discussion

The DU_SWAMP aeroservoelastic simulator was employed to evaluate the above distributed flap control system performance and validate the procedure for developing *aeroservoelastic computational models* for distributed control system design. The performance was tested with a 15 m/s wind condition in Region III. The three dimensional wind input is generated by TurbSim[9, 25] with 6% turbulence intensity generated according to the Kaimal spectrum. Six percent turbulence intensity is low compared to typical standards but is chosen in order to ensure the highest reliability of longer simulation runs by DU_SWAMP. During the control evaluation 400 second time segments were used.

Figure 8 shows the equivalent damage loading for the baseline PD contoller (top) from reference[9] and the current LQR flap controller design (bottom). The LQR controller design showed a 15.5 % reduction in fatigue damage equivalent laod and a 13.3% reduction in the standard deviation of the waveform. This is less then

the results found from,[9] however comparable to a conventional tip deflection rate feedack control design (see reference[10] for more details). Further investigation of combinations of system identification models, sensor measurements, and actuator types and locations can influence and change the performance of the control system as part of future work.

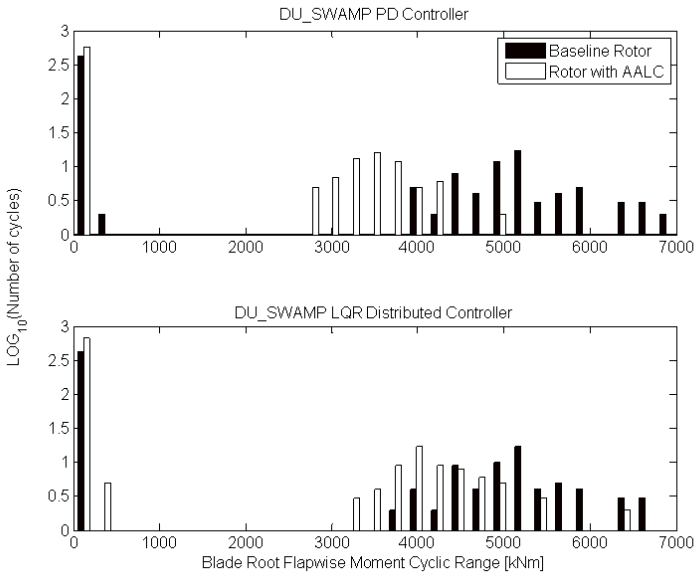

Figure 5. PD DEL (top) and LQR DEL (bottom) summarized results

Next, representative time domain responses are shown for the LQR flap controller design (given in blue) versus *without* flap control (given in red). The 5MW reference turbine example used in this paper demonstrates the overall control law design procedure for the MIMO LQR flap controller blade load reduction. Figure 6 shows reductions for the root moment (left) and blade flap local deflection (right) responses in comparison to no flap control. The LQR Flap controller results are shown in Fig. 7 for the flap control input

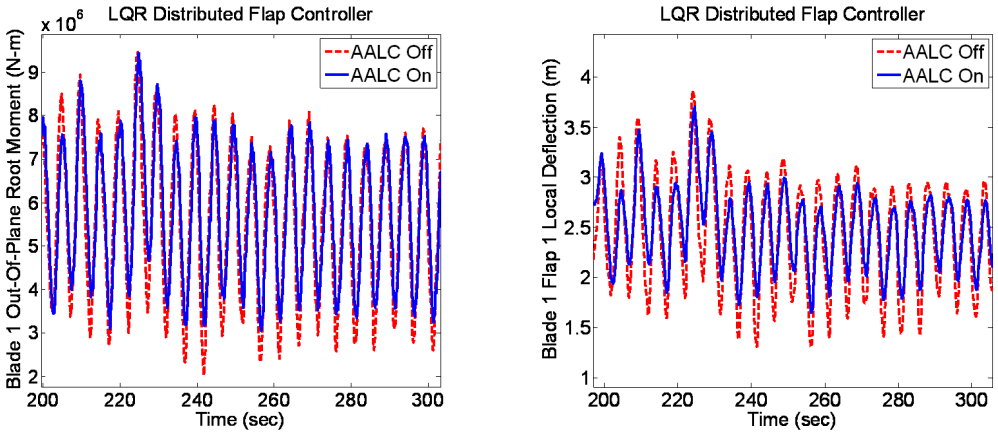

Figure 6. Blade 1 out-of-plane root moment response (left) and local deflection response (right) both with and without AALC, repsectively

(left) and the corresponding blade flap local deflection rate response (right). As a rule-of-thumb the flap deflection limit was kept to ± 10 degrees (see Fig. 1).

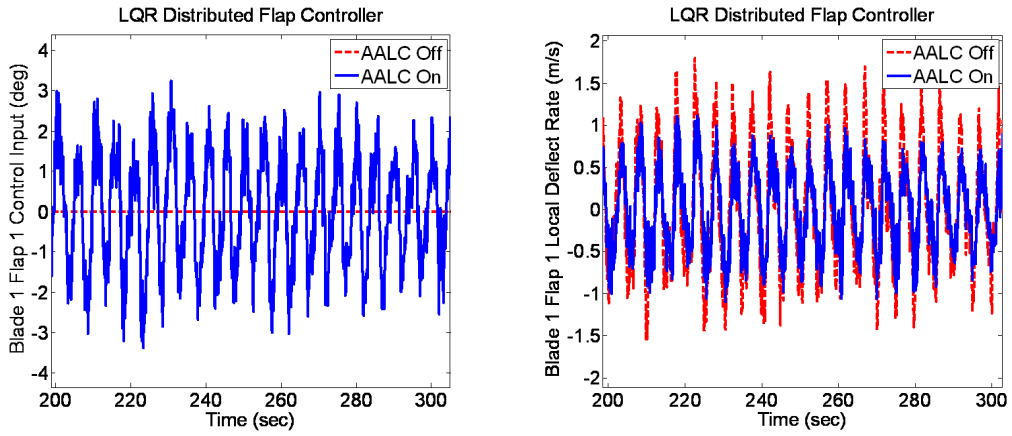

Figure 7. Blade 1 LQR controller input (left) and Local deflection rate response (right) both with and without AALC, repsectively

The diversity of DU_SWAMP allows for refinement of multiple flap inputs (see Fig. 8 left) along with the phasing for each blade flap inputs (as shown in Fig. 8 right). Future work will allow for custom load reduction profiling as a function of wind condtions such as high turbulence and gust scenarios. This will become increasingly more important as wind turbine blades continue to increase in length along with higher towers, containing multiple wind conditions along the span of each blade and each individual blade itself.

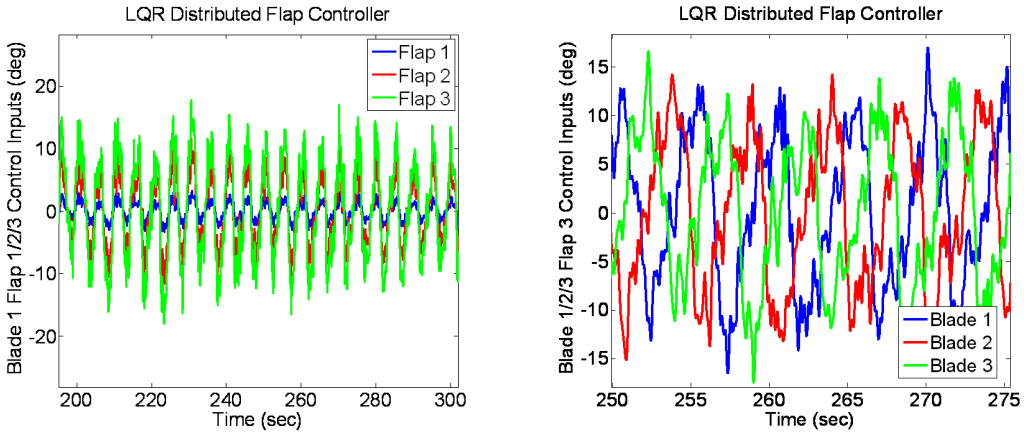

Figure 8. Blade 1 LQR controller input flaps 1/2/3 (left) and blade 1/2/3 flap 3 (right) inputs

V. Summary and Future Work

This paper has shown the feasibility for employing an integral system identification and modern controller design procedure for load reduction using multiple flap actuators and sensors along the blade. The NREL 5MW UpWind reference wind turbine was implemented in the high fidelity DU_SWAMP aeroservoelastic simulator. Numerical results demonstrated the proof-of-concept for the procedure and for the initial design. Future work will include the topic areas listed below.

First, techniques for system identification of the operational aeroservoelastic wind turbine in stochastic inflow need to be perfected. The work presented here has demonstrated need for thorough characterization of the operating, aerodynamically loaded wind turbine system. This is the first step in the process of understanding necessary system dynamics and then making appropriate choices regarding what to include in the implementation of a control scheme. The operational modes of the wind turbine are expected to

be different from what can be measured on the parked turbine system due to effects of rotor rotation and aerodynamic loads and damping. Measurement of the operational modes with the use of the appropriate rotor excitation will enable better controller design. Excitations may include, but are not limited to, individual flap actuations and blade pitch actuations. The nature of the ideal input signal for these actuations is still to be determined.

Second, in the context of control system design, the control performance is tied directly to the accuracy of the identified model. For identified state-space models that are compatible with a whole regime of MIMO modern control techniques (LQR, LQG, H_∞, μ-synthesis, loopshaping, uncertainty modeling, multivariable stability margins, etc. along with other robust control concepts) can now be applied. Many of these modern control design techniques are performed with respect to a performance index or cost function. The cost function can be designed for efficient and robust operation (with respect to a changing environment) of blade AALC strategies and integration with a *smart* health monitoring and overall wind turbine control system architecture.

Finally, further investigations of load reduction under varying wind conditions using distributed flaps and various combinations of sensor measurements can be assessed. Studies of multiple flaps, flap spanwise locations, and sensor measurements (structural: strain, strain-rate, tip deflection, accelerometers, etc. and aerodynamic: pressure, pitot-tube, etc.) can now be conducted to help identify promising active aerodynamic load control techniques. Trade-off studies of loads reduction and effects on energy capture will help develop the *smart* wind turbine system with optimized performance for the future.

Acknowledgments

Sandia National Laboratories is a multiprogram laboratory operated by Sandia Corporation, a Lockheed Martin Company, for the U.S. Department of Energy's National Nuclear Security Administration under contract DE-AC04-94AL85000.

References

[1]McCoy, T.J. and Griffin, D.A., "Active Control of Rotor Geometry and Aerodynamics: Retractable Blades and Advanced Devices," AWEA WINDPOWER 2007 Conference, Los Angeles, Ca., June 4-6, 2007.

[2]Yen, D., van Dam, C.P., Smith, R.L. and Collins, S.D., "Active Load Control for Wind Turbine Blades Using MEM Translational Tabs," Proceedings of the 2001 ASME Wind Energy Symposium (AIAA 2001-0031), Reno, Nevada, January 2001.

[3]Yen Nakafuji, D.T., van Dam, C.P., Michel, J., Morrison, P. "Load Control for Turbine Blades: A Non-Traditional Microtab Approach," Proceedings of the 2002 ASME Wind Energy Symposium (AIAA 2002-0054), Reno, Nevada, January 2002.

[4]van Dam, C.P., et. al., "Computational and Experimental Investigation into the Effectiveness of a Microtab Aerodynamic Load Control System," unpublished Sandia Report, August, 2004.

[5]Andersen, P.B., et. al., "Integrating Deformable Trailing Edge Geometry in Modern Mega-Watt Wind Turbine Controllers," EWEA 2008 EuropeanWind Energy Conference & Exhibition, Belgium, March 31 - April 3, 2008.

[6]Barlas, T.K. and van Kuik, G.A.M., "State of the Art and Prospectives of Smart Rotor Control for Wind Turbines," The Science of Making Torque from Wind, J. of Physics: Conference Series 75, 2007.

[7]Barlas, T.K. and van Kuik, G.A.M., "Aeroelastic Modelling and Comparison of Advanced Active Flap Control Concepts for Load Reduction on the UpWind 5MW Wind Turbine," European Wind Energy Conference & Exhibition, Marseille, France, 16-19, March, 2009.

[8]MatLab/Simulink - Matlab version 7.8 release 2009a and Simulink version 7.3 release 2009a. The Mathworks Inc.

[9]Resor, B.R., Wilson, D.G., Berg, D.E., Berg, J.C., Barlas, T.K., and vanKuik, G.A.M., "Impact of Higher Fidelity Models on Simulation of Active Aerodynamic Load Control for Fatigue Damage Reduction," AIAA Aerospace Sciences Meeting and Exhibit, Orlando, Florida, Jan. 4-7, 2010.

[10]Wilson, D.G., Berg, D.E., Barone, M.F., Berg, J.C., Resor, B.R., and Lobitz, D.W., "Active Aerodynamic Blade Control Design for Load Reduction on Large Wind Turbines," European Wind Energy Conference & Exhibition, Marseille, France, 16-19, March, 2009.

[11]Berg, D.E., Wilson, D.G., Berg, J.C., Resor, B.R., Barone, M.F., Zayas, J.R., Kota, S., Ervin, G., and Maric, D., "The Impact of Active Aerodynamic Load Control on Wind Energy Capture at Low Wind Speed Sites," European Wind Energy Conference & Exhibition, France, 16-19, March, 2009.

[12]Berg, D.E., Wilson, D.G., Resor, B.R., Barone, M.F., Berg, J.C., Kota, S. and Ervin, G., "Active Aerodynamic Blade Load Control Impacts on Utility-Scale Wind Turbines," WINDPOWER 2009, Chicago, Illinois, 5-7 May, 2009.

[13]Wilson, Berg, D.E., D.G., Resor, B.R., Barone, M.F., and Berg, J.C., "Combined Individual Pitch Control and Active Aerodynamic Load Controller Investigation for the 5MW UpWind Turbine," WINDPOWER 2009, Chicago, Illinois, 5-7 May, 2009.

[14]Wilson, D.G., Berg, D.E., Lobitz, D.W., and Zayas, J.R., "Optimized Active Aerodynamic Blade Control for Load Alleviation on Large Wind Turbines," WINDPOWER 2008 Conference & Exposition, Houston, Texas, June 1-4, 2008.

[15]Jonkman, J., Butterfield, S., Musial, W., Scott, G., "Definition of a 5MW Reference Wind Turbine for Offshore System Development," National Renewable Energy Laboratory, NREL/TP-500-38060, February 2009.

[16]Horta, L.G., Phan, M., Juang, J.-N., Longman, R.W., and SUlla, J., "Frequency Weighted System Identification and Linear Quadratic Controller Design," Proceedings of the AIAA Guidance, Navigation and Control Conference, New Orleans, Louisiana, Aug. 1991, pp. 1172–1179.

[17]Bialasiewicz, J.T. and Osgood, R.M., "Advanced System Identification Techniques for Wind Turbine Structures," 1995 SEM Spring Conference, Grand Rapids, Michigan, June 12-15, 1995, (NREL/TP-442-6930).

[18]Dumitrache, A. and Botez, R., "Active Control Laws for Aeroelasticity," Proceedings of Applied Mathematics and Mechanics, 5, pp. 651–652 (2005) / DOI 10.1002/pammm.200510302.

[19]Newsom, J.R., Robertshaw, H.H., and Kapania, R.K., "Control Law Design in a Computational Aeroelasticity Environment," AIAA 2003-1415, 44^{th} AIAA/ASME/ASCE/AHS Structures, Structural Dynamics, and Materials Conference, 7-10 April 2003, Norfolk, Virginia

[20]Juang, J.-N. and Pappa, R.S., "An Eigensystem Realization Algorithm for Modal Parameter Identification and Model Reduction," Journal of Guidance, Control and Dynamics, Vol. 8, No. 5, Sept.-Oct., 1985, pp. 620–627.

[21]Juang, J.-N., *Applied System Identification*, Prentice Hall PTR, Upper Saddle River, NJ, 1994.

[22]Juang, J.-N., Horta, L.G., and Phan, M., "User's Guide for System/Observer/Controller Identification Toolbox," NASA Technical Memorandum 107566, 1992.

[23]Elkaim, G.H. "System Identification-Based Control of an Unmanned Autonomous Wind-Propelled Catamaran," Control Engineering Practice 17 (2009), pp. 158–169.

[24]Bryson, Jr., A.E. and Ho, Y.-C., *Applied Optimal Control*, Hemisphere Publishing Corp., New York, 1975.

[25]NWTC Design Codes (TurbSim by Neil Kelley and Bonnie Jonkman), http://wind.nrel.gov/designcodes/preprocessors/turbsim/. Last modified 11-September-2008; accessed 11-September-2008.